

2D modeling and pre-stack depth migration of Husky line H98-154

Hesham M. Moubarak, John C. Bancroft and Don C. Lawton

ABSTRACT

2D forward numerical seismic modeling of a complex geology structure was used in this experiment to optimize the acquisition parameters and to aid in the seismic interpretation. Synthetic seismic data were acquired for a numerical model of a fault-fold structure encountered in North Eastern British Columbia. These synthetic shot gathers are used to investigate which migration algorithms would produce the best images in such complex environments. Results have shown that the pre-stack depth migration from the topography with the known velocity model have yielded the optimum migrated image. Acoustic and elastic numerical modeling techniques were used to simulate waves propagating in the complex medium, and the most difficult structural styles to image were investigated.

INTRODUCTION

Numerous modeling approaches can be distinguished, using assumptions regarding the seismic data and subsurface structures, in an attempt to simulate the seismic response to the subsurface structures. One of those approaches that can be used is prestack depth Kirchhoff migration using first-arrival traveltimes. However, this approach has been shown to produce poor images in areas of complex structures. To avoid this problem, we used a vector wave migration Kirchhoff operator method which uses a new type of time field calculations, called the maximum energy time field, that allows these models to be closer to real geological conditions. The maximum energy traveltime calculation method was proposed by Dave E. Nichols (1996) in his work "Maximum energy traveltimes calculated in the seismic frequency band" for calculating the traveltimes that estimate the traveltime of the maximum energy arrival, rather than the first arrival. This method estimates a traveltime that is valid in the seismic frequency band, but not in the usual high-frequency approximation. In other words, instead of solving the Eikonal equation for the traveltime, solving the Helmholtz equation to estimate the wavefield for a few frequencies, then performing a parametric fit to the wavefield to estimate a traveltime, amplitude, and phase. The images are created using these parameters (See Figure 15 as an example of using maximum energy time field method using only 23 shots at the surface). In a Kirchhoff imaging algorithm the method can be comparable in quality to those created using a full-wavefield and finite difference migration.

STUDY LOCATION:

The Muskwa Area is located North Eastern British Columbia (NTS 94B), approximately 250 km NW of Fort St. John, B.C. This area has a deformation pattern dominated by box folds, along with fault propagation folds and complicated multiple detachment surfaces. The target reservoir is the Mississippian age Debolt formation fractured carbonates. (See Figure 1)

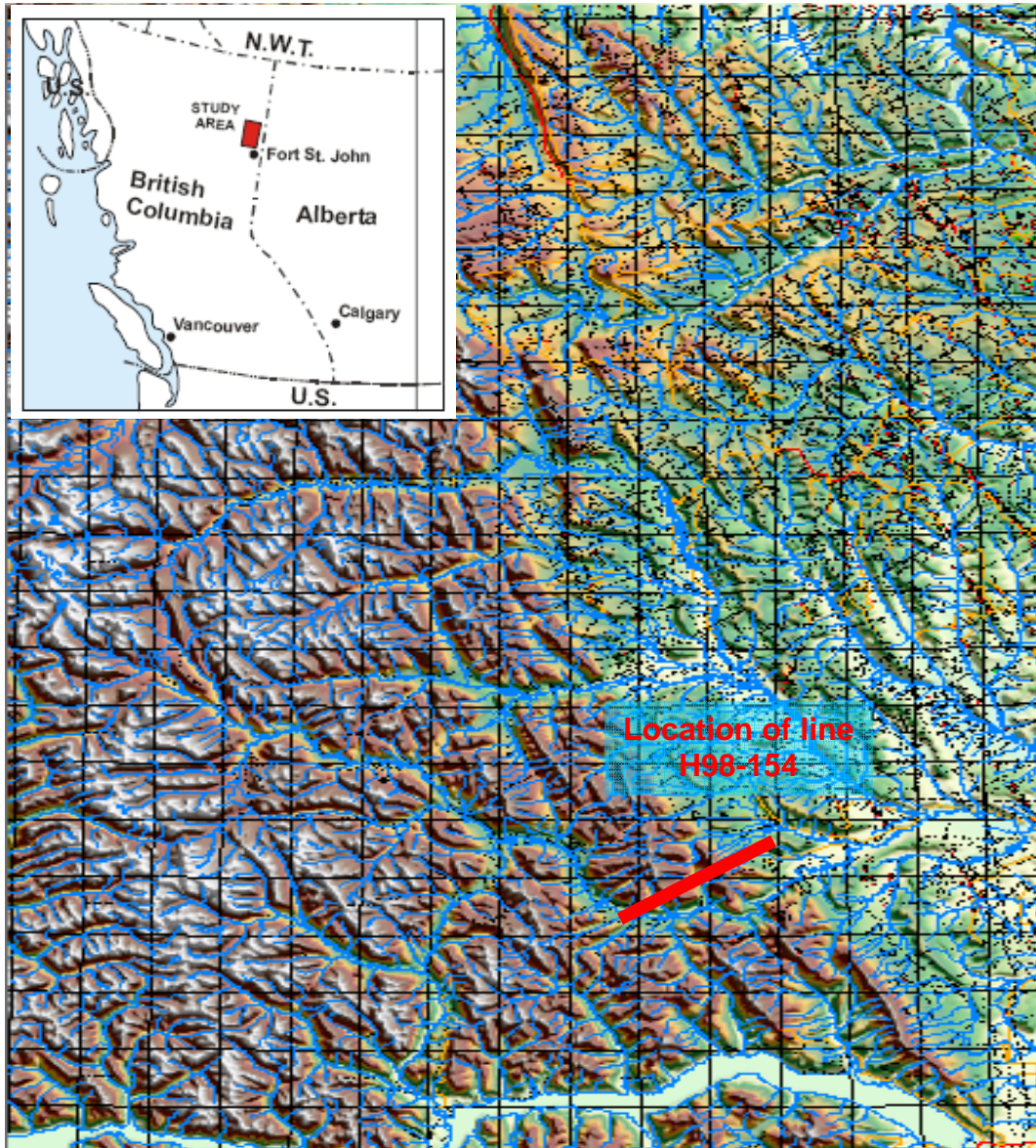
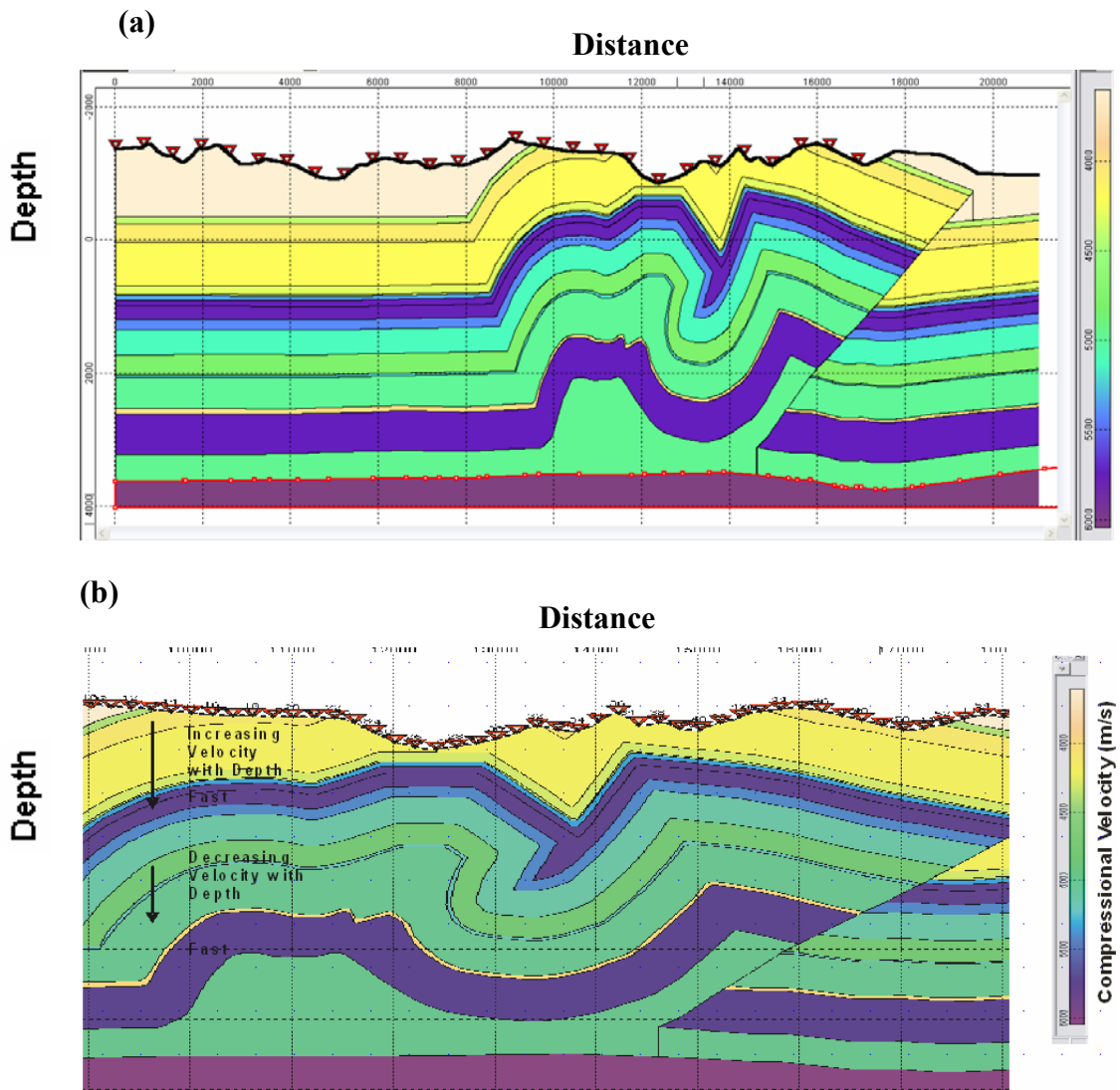


FIG. 1. Study location (courtesy of David Emery, Husky Energy).

MODEL BUILDING

A geologic/velocity model with section length 25 km and section depth 6km was built, based on well information and geological interpretation of the seismic line H98-154, which was extended to the east; and the structural complexity was removed on the west. After balancing and restoration of the geologic model three models were created: a compressional velocity model, where interval velocities range between 3600-6050 m/s; a shear velocity model where interval velocities range between 1500-3551m/s; and a density model where densities range between 2-2.67 kg/m³. One can notice the rough topography, difficult velocity structure (increasing velocity with depth in the shallow layers, followed by fast layers that are seated over layers with decreasing velocity in the deeper part of the model). Also, an anticline on the west of the model, central syncline with different degrees of dipping – a challenge to image in this study- and a fault environment in the east part of the model. The model was based on the structures in a carbonate rock formation of Paleozoic age. (Figure 2).



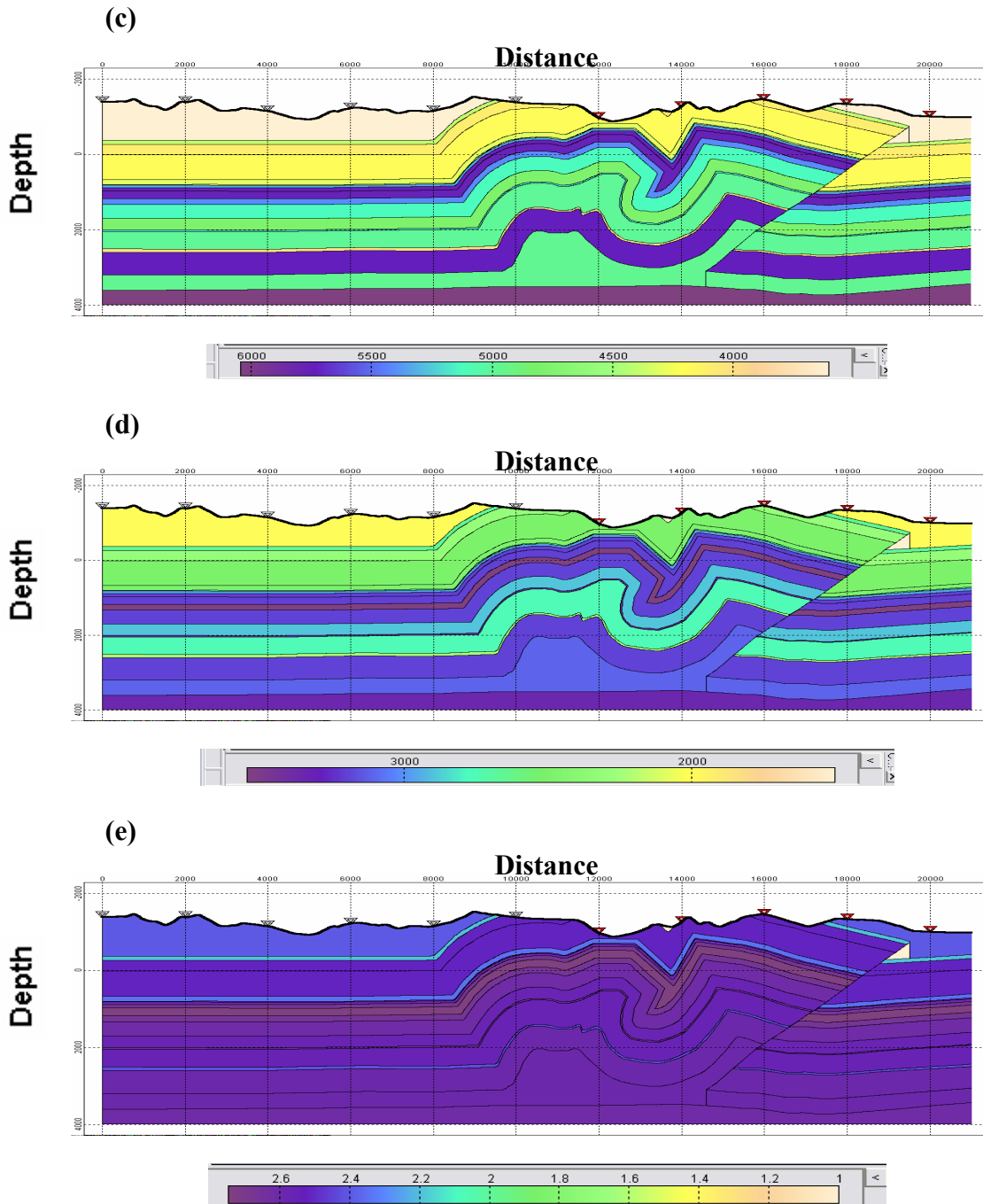


FIG. 2. (a). LithoTech Balanced Geologic/velocity Model of northeastern British Columbia, created from the seismic line H98-154, using the velocities from five wells on or near the line which is expanded to the east and the structural complexity removed on the west to help in imaging. (Courtesy of Larry Mewhort, David Emery, Bart Scout, Husky Energy). (b). Geologic Model which represents the seismic line. (c). Compressional velocity model where velocities range 3600-6050 m/s, section length = 25 km, section depth = 6 km. (d). Shear velocity model where velocities range 1500-3551 m/s, , section length = 25 km, section depth = 6 km. (e). Density model where densities range from 2-2.75 kg/m³, , section length=25 km, section depth=6 km.

Surface Geology of Line H98-154:

The eastern two-thirds of this line has a surface cover of early Cretaceous clastics (increasing seismic velocity with depth), while the western third of the line is covered by Triassic carbonates and calcareous siltstones and shales (constant velocity laterally, decreasing velocity with depth). There are five wells on or near the seismic line. (See Figure 3)

The five wells are (Wells 3, 4, 5 have the same name):

1. C-029-E/094-B-08 was drilled in 1962 then abandoned.
2. D-030-E/094-B-08 was drilled in 1996 and still producing.
3. B-004-H/094-B-07 was drilled in 1998 then abandoned.
4. B-004-H/094-B-07 was drilled in 1999 then abandoned.
5. B-004-H/094-B-07 was drilled in 2000 then shut in.

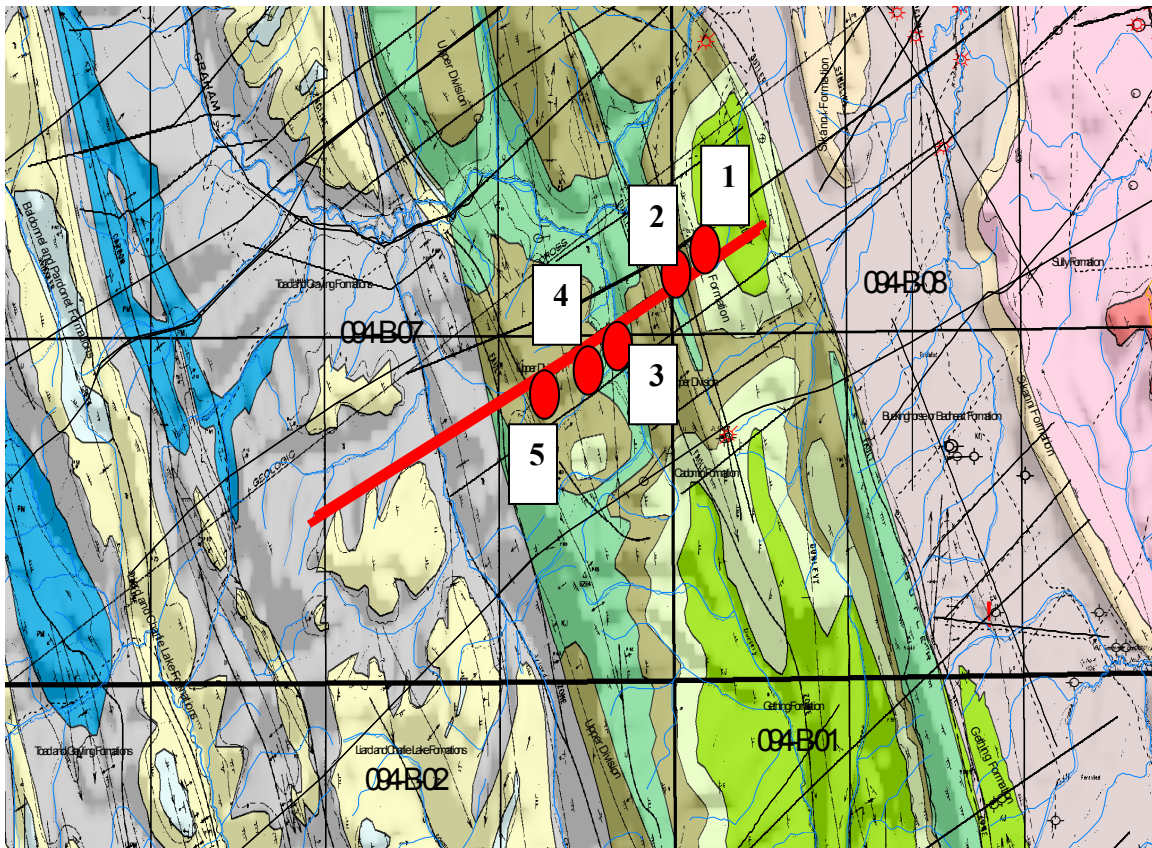


FIG. 3. Surface Geology of Line H98-154, (courtesy of David Emery, Husky Energy).

Table 1. Physical parameters used in the model (Vp: Compressional velocity in m/s, Vs: Shear velocity in m/s, ρ : Density in kg/m³) (Courtesy of David Emery, Husky Energy).

Formation	Lithology	Vp (m/s)	Vs (m/s)	ρ (kg/m ³)
Fort St. John	Marine shale; sandstones	3600	2000	2.4
Gething	conglomerate and sandstone.	4400	2671	2.2
Beattie Peak	Mudstone, shaly siltstone and sandstone	4100	2313	2.52
Monteith Formation	Fine grained argillaceous sandstone.	4200	2499	2.52
Fernie	Marine shale.	4300	2485	2.35
Nordeg	Black cherty and phosphate limestones.	4350	2683	2.57
Pardonet	Carbonaceous-argillaceous limestone.	5340	2967	2.6
Baldonnel	Limestone, minor dolomite; interbedded siltstones	5770	3206	2.67
Charlie Lake	Dolomitic to calcareous sandstone, siltstone, sandy limestone, dolostone.	5780	3211	2.75
Halfway	Calc or dolomitic sandstone.	5420	3551	2.67
Doig	Dark calcareous shale.	5130	3201	2.62
Montney	Calcareous siltstone, silty limestone and silty shale.	4780	2899	2.57
Belloy	Sandy dolostones.	5200	3361	2.64
Kiskatinaw	At its base is generally a quartz sandstone. Above these sandstones the lithology is more varied, with shales.	5000	2757	2.56
Golata	Limestone, dark shale and sandstone.	4000	2226	2.43
Debolt	Limestone.	5750	3200	2.6
Banff	Silty limestone and calc shale.	4980	3121	2.6
Wabamun	Dark grey dolostone and limestone	6050	3361	2.62

Imaging Problems in the Model

Eight regions of illumination (See Figure 4) have been selected to be studied carefully by using first arrivals and maximum energy time field calculations.

Regions C, and H have been fully imaged, while location F is only partially imaged. However, the other five regions (A, B, D, E, and G) have not been imaged successfully. The model was expanded a few kilometers to the west and the number of shots increased as a first step to tackle the problem. Imaging of dips greater than 30° appears to be a problem so far, along with imaging of the central syncline between the box-fold on the west and the fault propagation fold on the east (See Figures 4 and 17).

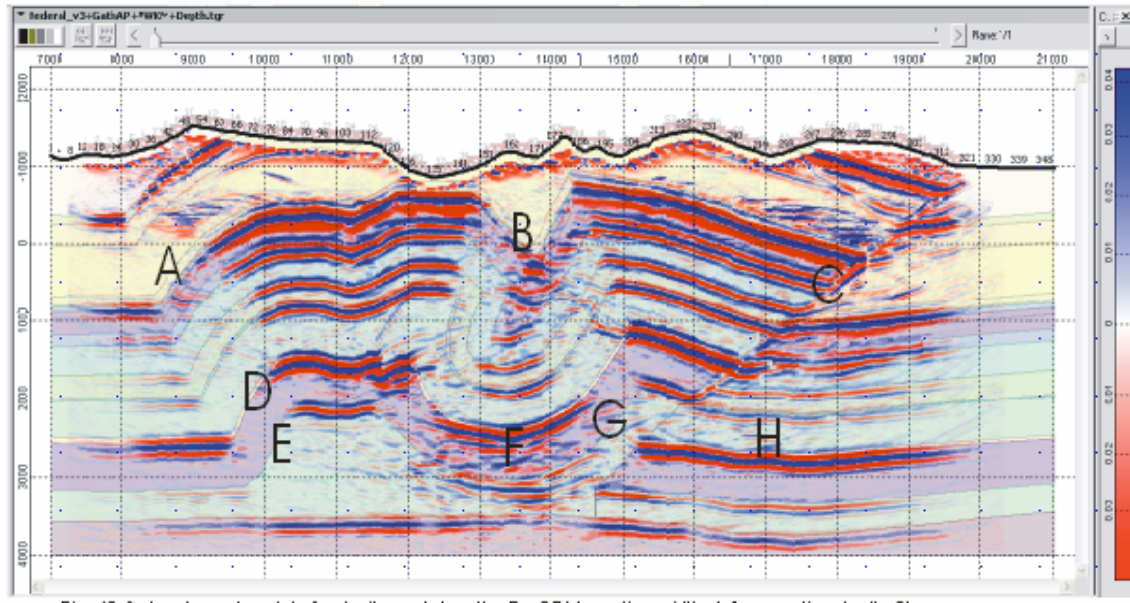


FIG. 4. Colored-overlay plot of the velocity model on the PreSDM. Section length = 14 km, section depth = 6 km. Shown are eight regions of interest and the capability of imaging.

Table 2. Locations of formations.

Locations	Formations	
		A- Fold edge
A, B, C	Baldonnell	B- Syncline structure
		C- Thrust Faults
D	Debolt (Fold edge)	
E, F,G	Parts of syncline structure	
H	Thrust Fault	

Illumination Concerns

The near surface geological complexity creates a limited illumination aperture for imaging the subsurface geology. Also, we have poor imaging when the near surface has an inverted velocity profile (decreasing velocity with depth). In addition there is the effect of the high velocity carbonates on both the downgoing and upgoing wave paths.

Effects of high frequency can be seen on Figure 6 near the surface, but the reflection distortions are healed in deeper layers. Pre-stack depth migration using acoustic modeling with 15 Hz Ricker wavelet and 25 Hz Ricker wavelet, first arrival travel times, and maximum energy travel time has partially imaged the steep dipping strata (See Figures 5, 6, 7, 8).

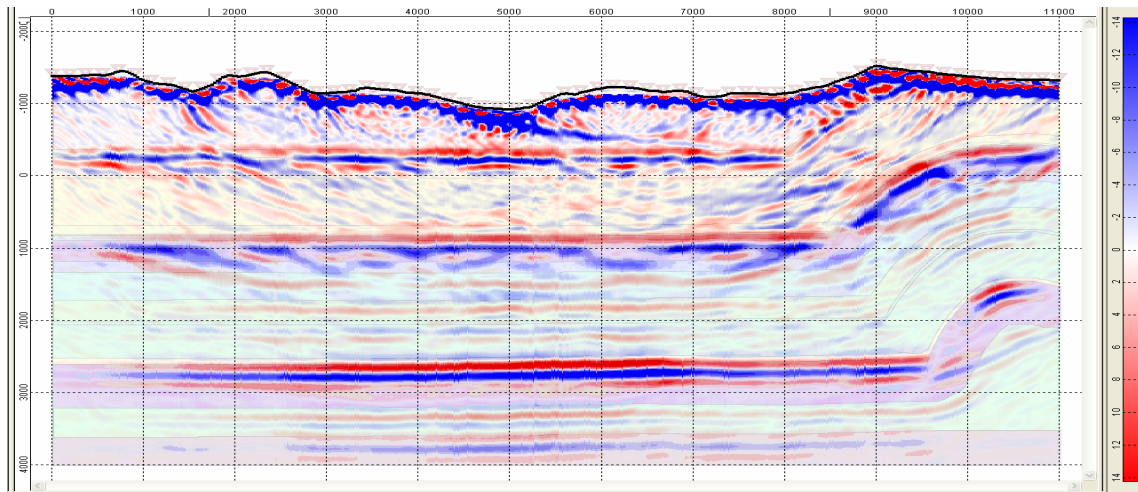


FIG. 5. PreSDM using Acoustic Modeling-First Arrival, 15 Hz Ricker wavelet- 62 Shots w/180m interval-11km, Elapsed Time to create Shot gathers, time field, snapshots 08:00:46. Elapsed time for migration: 09:10:08.

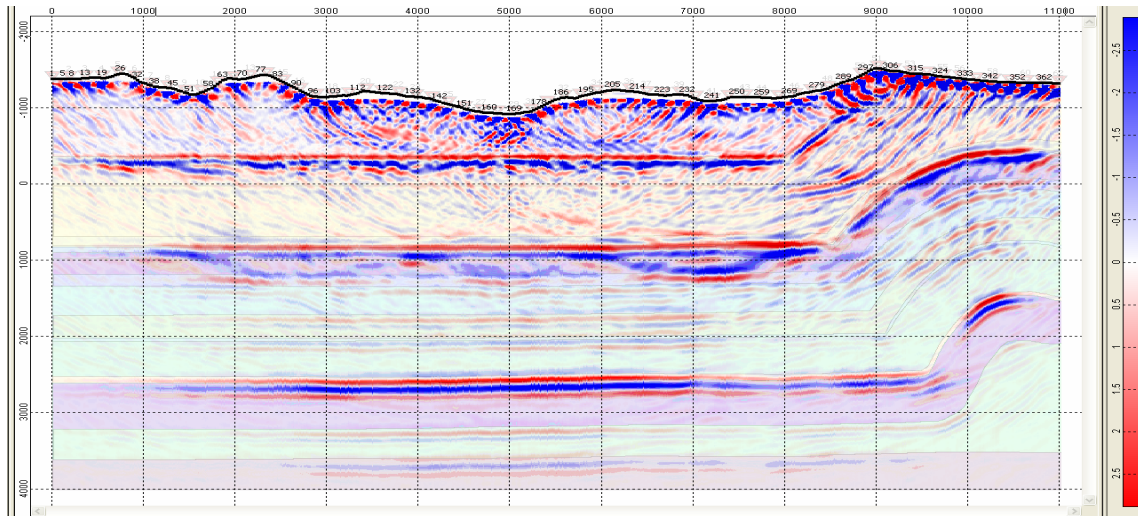


FIG. 6. PreSDM using Acoustic Modeling-First Arrival, 25 Hz Ricker wavelet- 62 Shots w/180m interval - 11 km, Elapsed Time to create shot gathers, time field, snapshots 27:47:48. Elapsed time for migration: 09:44:30 (Extra half an hour).

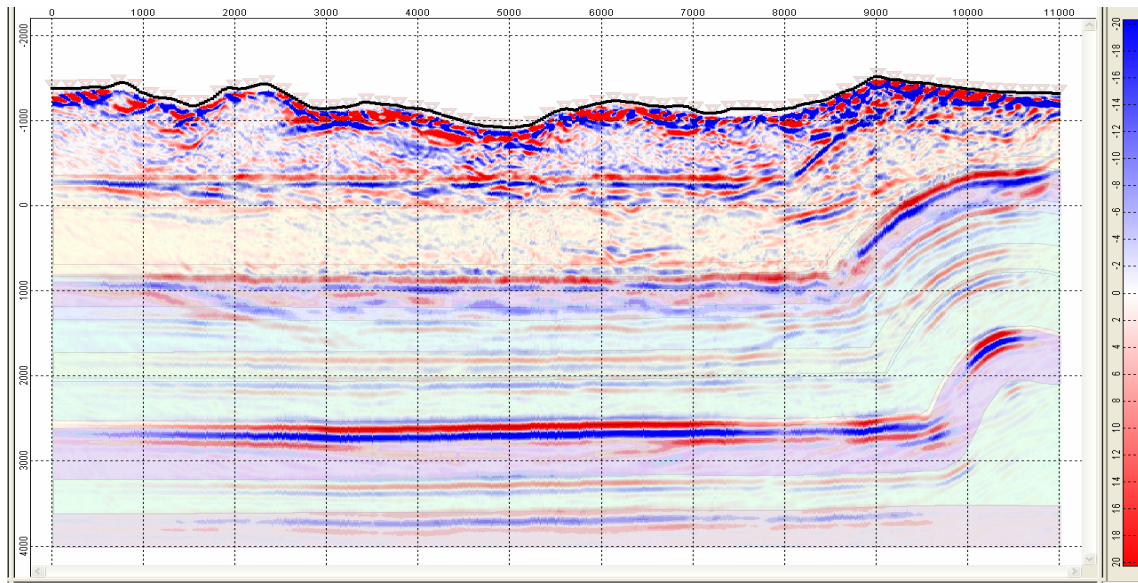


FIG. 7. PreSDM using Acoustic Modeling-Maximum Energy, 25 Hz Ricker wavelet-62 Shots w/180m interval - 11 km, Elapsed Time to create shot gathers, time field, snapshots 33:24:26. Elapsed time for migration: 09:40:40.

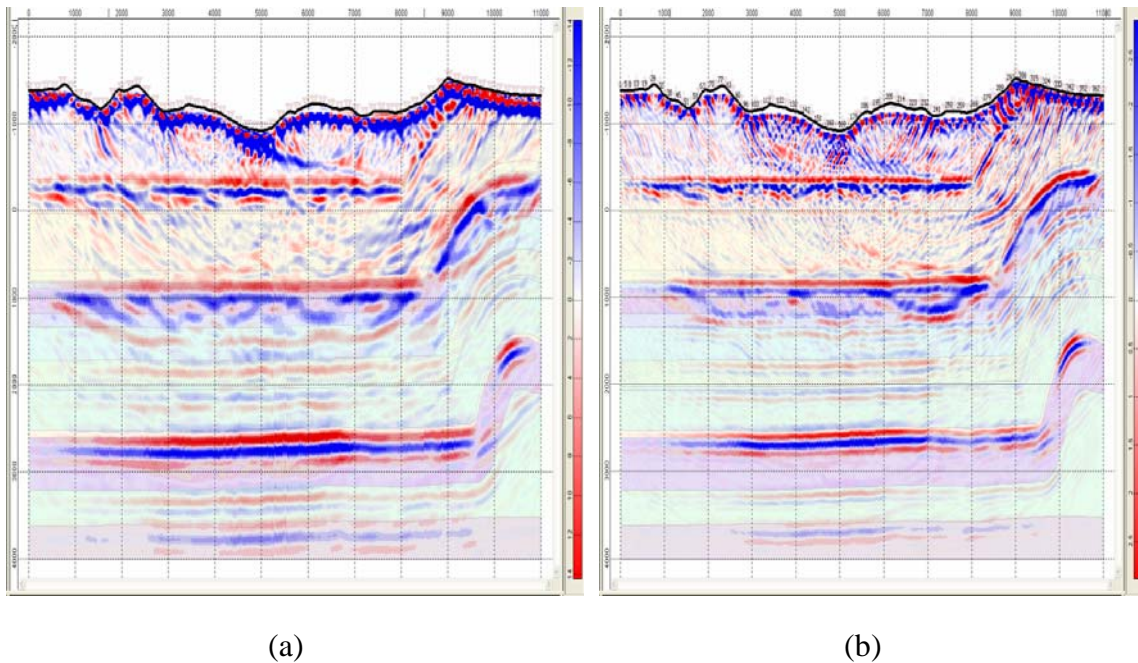


FIG. 8. Comparison between Pre-stack depth migration using the acoustic modeling with 15 Hz Ricker wavelet and 25 Hz Ricker wavelet. a) PreSDM using Acoustic Modeling-First Arrival, 15 Hz Ricker wavelet- 62 Shots w/180m interval - 11 km, Elapsed Time to create Shot gathers, time field, snapshots 08:00:46. Elapsed time for migration: 09:10:08. b) PreSDM using Acoustic Modeling-First Arrival, 25 Hz Ricker wavelet- 62 Shots w/180m interval - 11 km, Elapsed Time to create shot gathers, time field, snapshots 27:47:48 Elapsed time for migration: 09:44:30 (Extra half an hour)

WAVE JOURNEY

Snapshots of the propagating waves can be used as a tool to identify the events on the shot gathers, and in the following example, one can see that the propagating waves lasted one second to be recorded at the surface and yield info about the strata. Notice the amplitude decay at the steepest dips. One shot was run from topography using both acoustic and elastic modeling (Figure 9b), and its computation time and memory requirements were recorded (Figure 9c). Elastic modeling was almost three and a half times slower than acoustic modeling, requiring twice as much disk space as the acoustic modeling experiment.

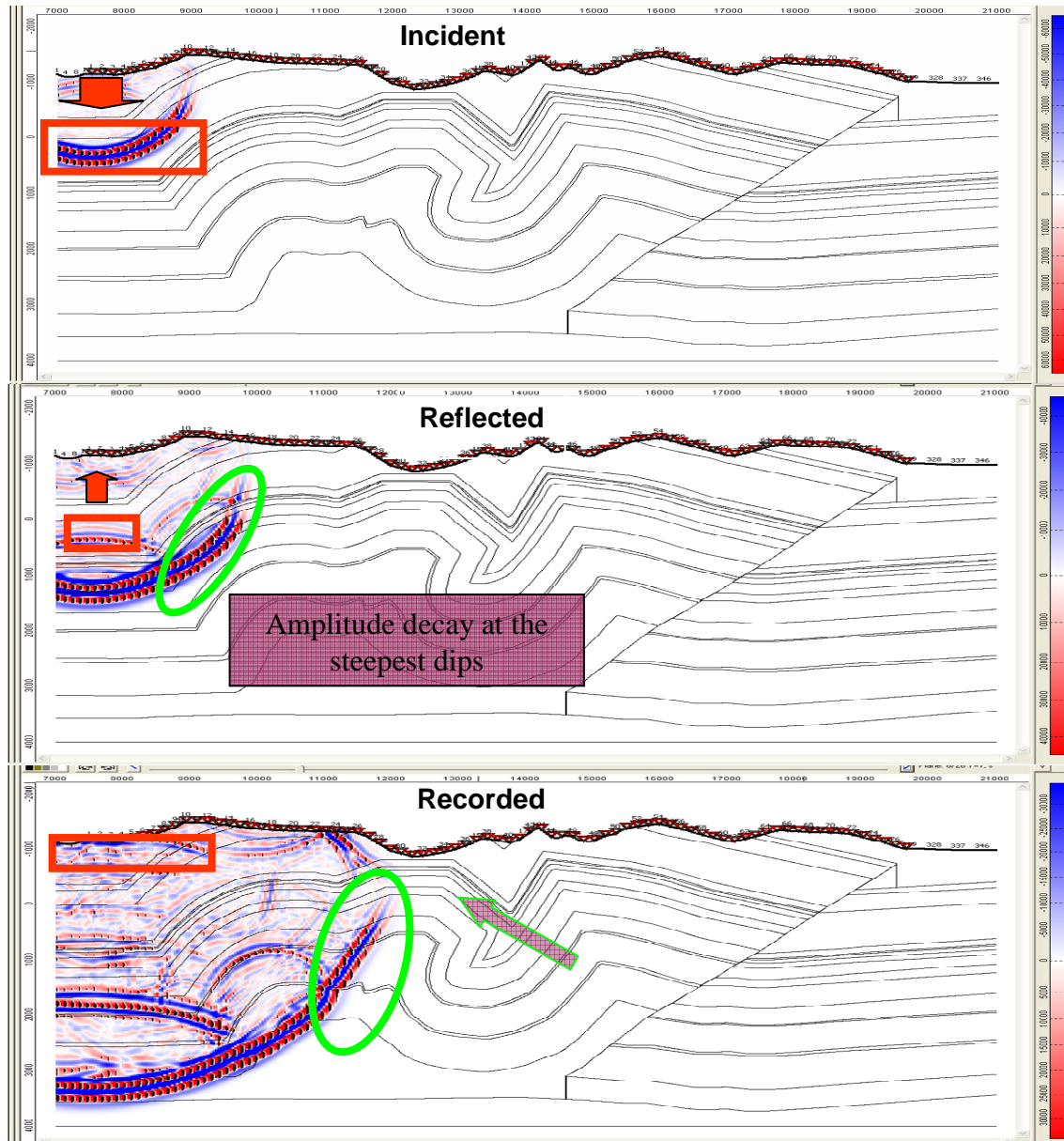


FIG. 9a. Snapshots of Propagating Incident, reflected, and recorded waves.

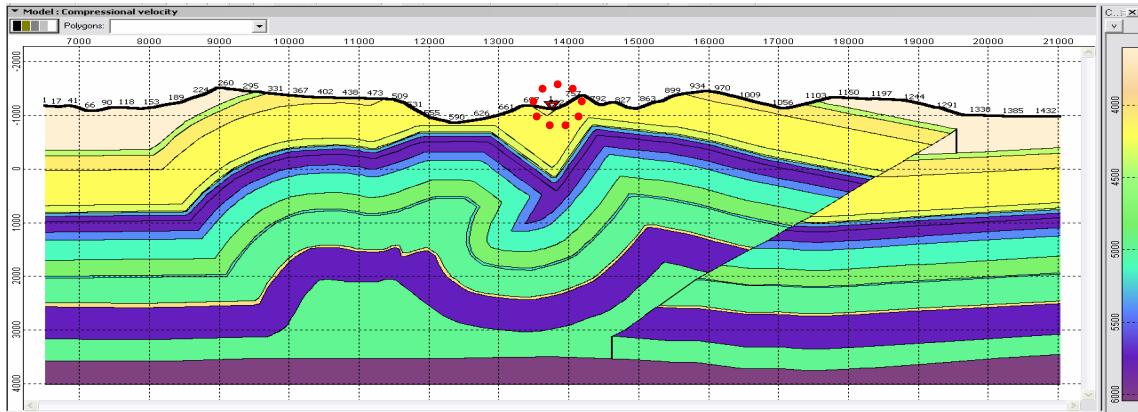
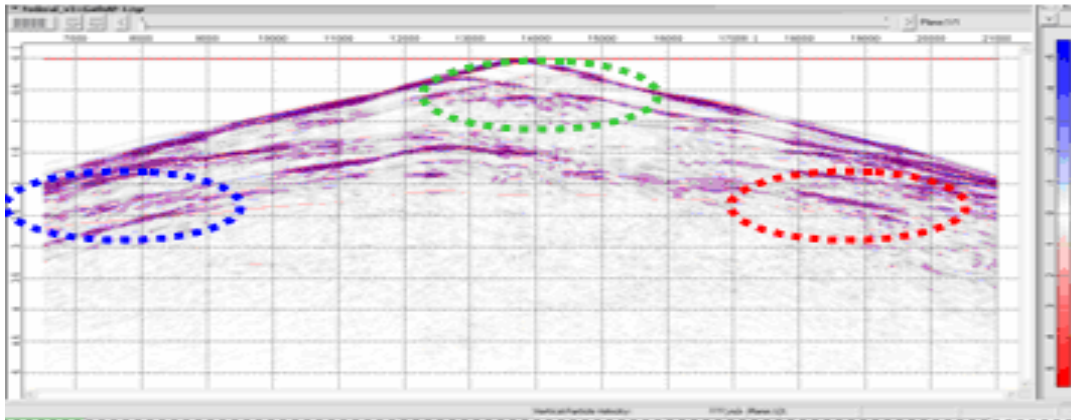
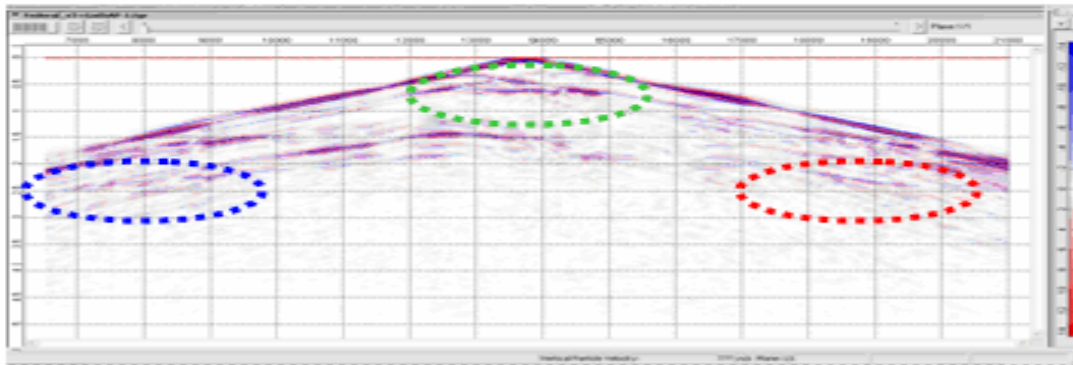


FIG. 9b. One shot run from topography using acoustic/elastic modeling.

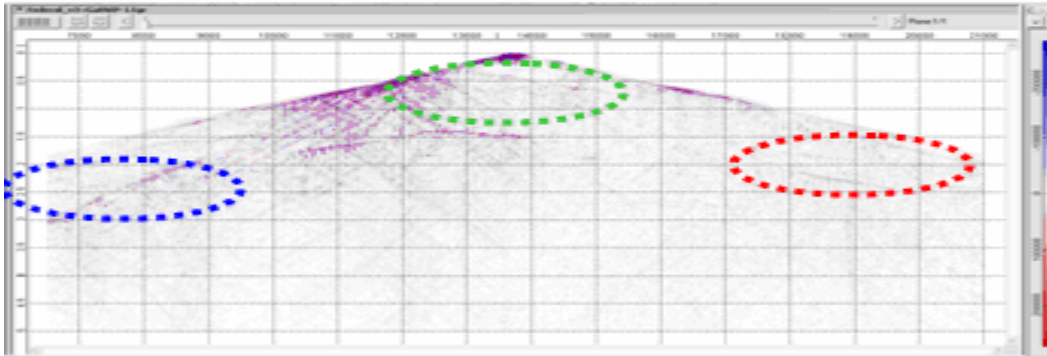
Acoustic Modeling
 One shot – 25 Hz Ricker wavelet
 Elapsed Time: 00:16:20 (3.2 times)
 Memory: 27 Mb (2.4 times)



Acoustic Modeling
 One shot – 15 Hz Ricker wavelet
 Elapsed Time: 00:05:47
 Memory: 11.1 Mb



Elastic Modeling
One shot – 25 Hz Ricker wavelet
Elapsed Time 01:36:12 (3.4 times)
Memory: 64 Mb (2.5 times)



Elastic Modeling
One shot – 15 Hz Ricker wavelet
Elapsed Time: 00:28:19
Memory: 25.6 Mb

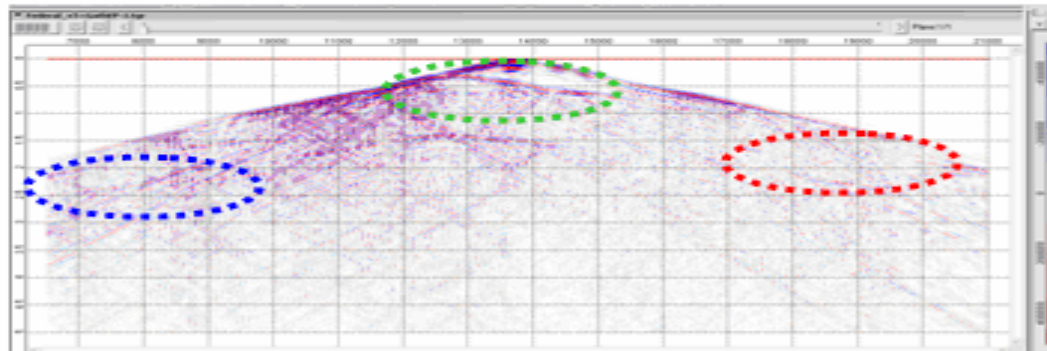
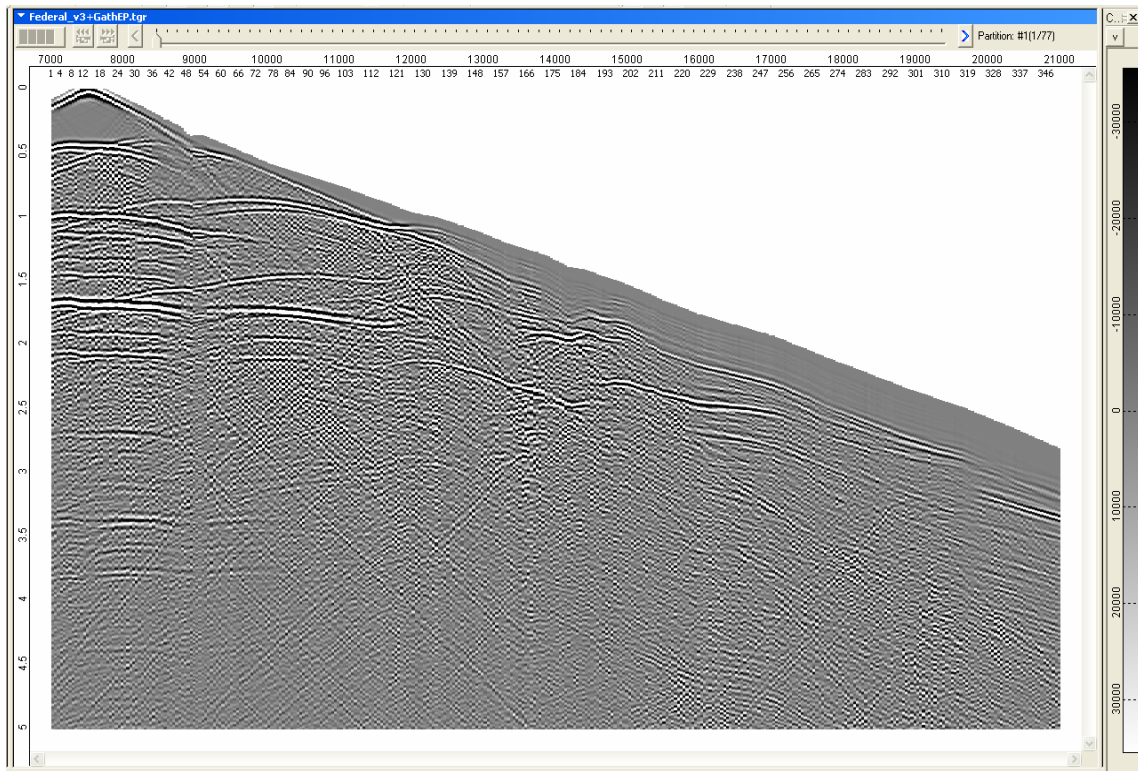


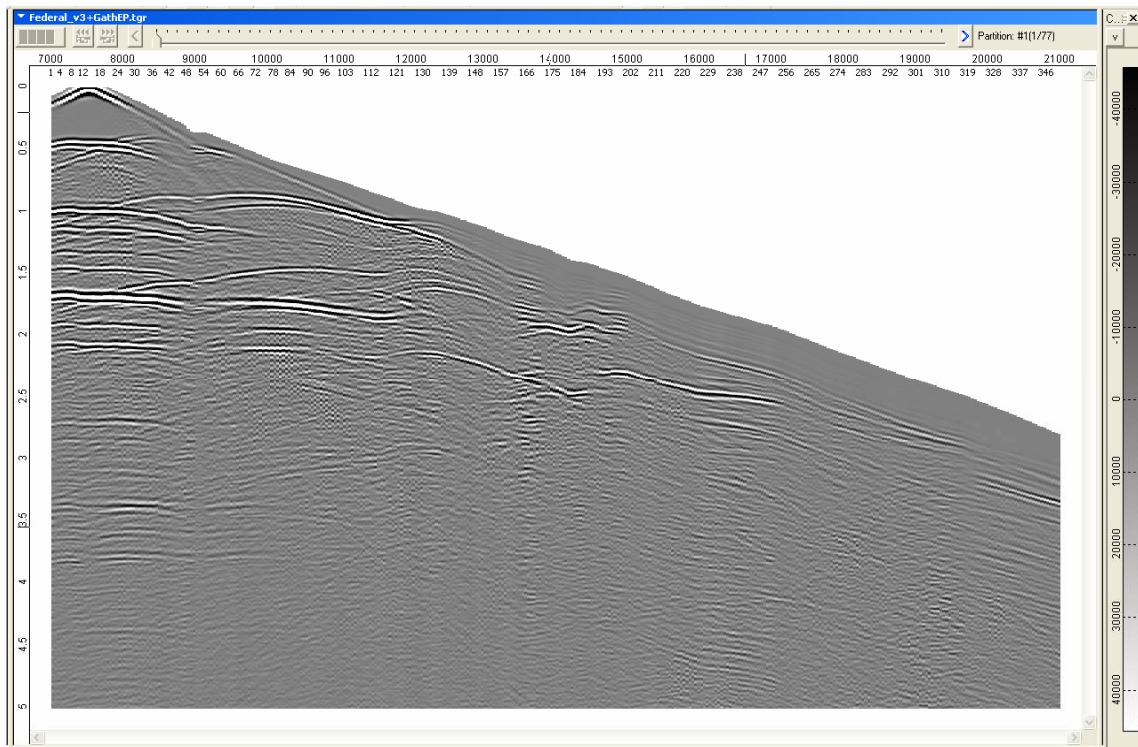
FIG. 9c. Result of running acoustic/elastic modeling on one shot from Figure 9b.

SINGLE GEOPHONE VERSUS GEOPHONE ARRAY

In the field we may regard the seismic system as being composed of three subsystems, a source or array of sources, an array of receivers, and the recording instrument. Each subsystem has numerous variables that we can adjust, as well as limitations we have to observe. There are many reasons for using multiple geophones, such as: electrical, vertical stack, spatial anti-alias filter, and attenuation of coherent noise. Part of this project is to optimize the acquisition parameters and to see how changing the geophone grouping and interval can act as a spatial anti-alias filter. The signal to noise ratio was enhanced when using an array of geophones instead of single geophone (Figure 10). By adding one percent noise, some events were visible as shown on the shot gather, and this scenario can be seen on the real seismic profile, especially in the zone on the western part of the line. (Figure 11)

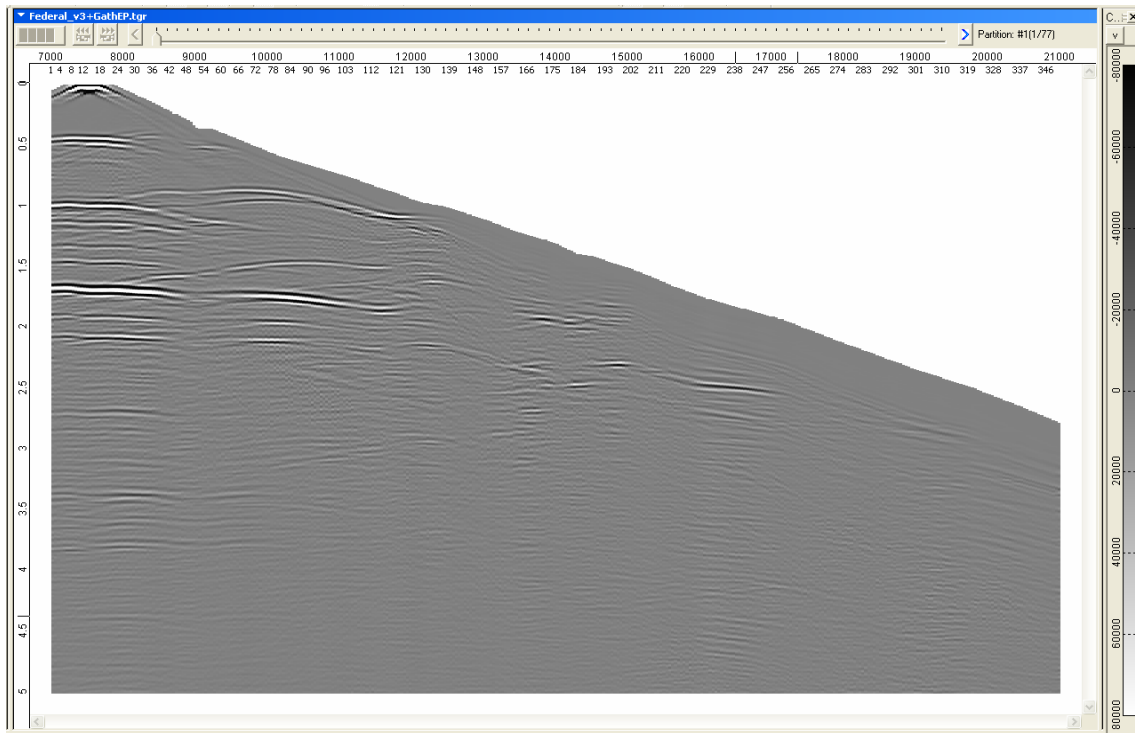


Single receiver

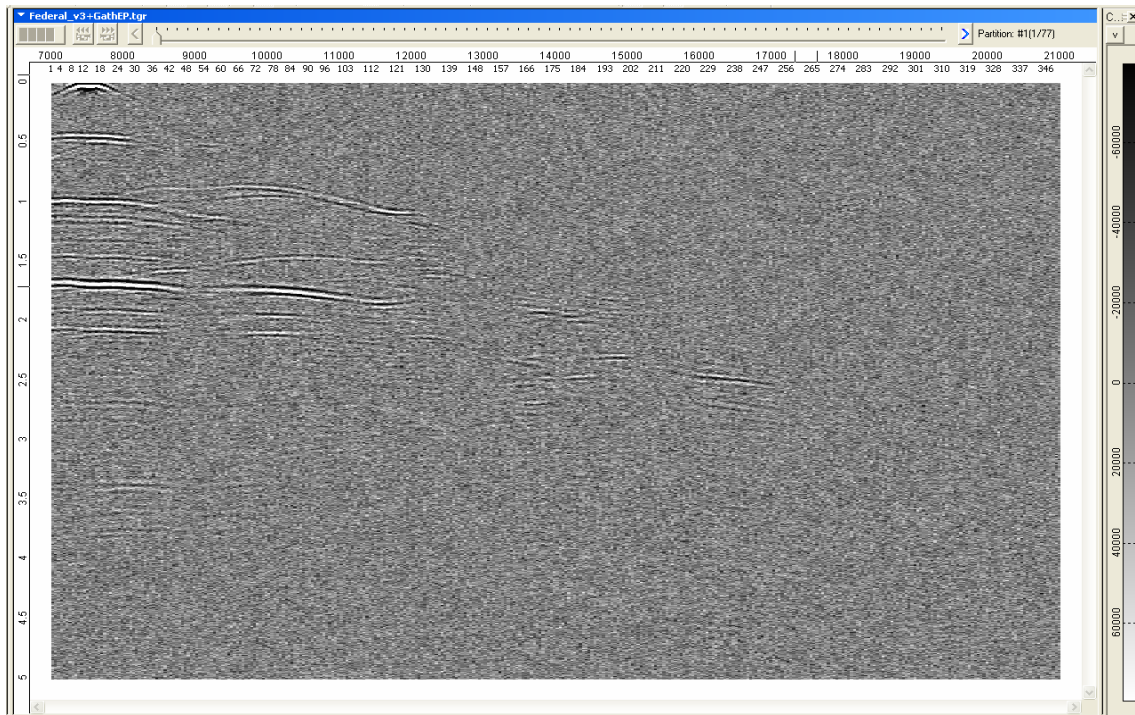


Group Traces: 3 Receivers, Interval: 3m

FIG. 10. Comparison between single to array geophone string.



Group Traces: 7 Receivers, Interval 3m without Noise



Group Traces: 7 Receivers , Interval 3m with White Noise: 1%

FIG. 11. Group Trace: 7 with and without white noise.

CALCULATION OF A TIME FIELD AND GREEN'S FUNCTION

Using a vector wave migration within the Tesseral modeling software, the time field produced will take into account that all waves exist in the synthetic shot gathers. Therefore, the first arrivals and maximum energy time field along with the energy field (Green function) have been calculated. (Figures 12 and 13). The general shape of the deeper formations can be noticed (Figure 13b).

“First Arrivals” are similar to the Eikonal Equation approach but it takes into account all of the modeled wave effects. “Maximum Energy” time field will be formed based on an incident wave maximum energy, and this makes the Kirchhoff operator also a maximum energy.

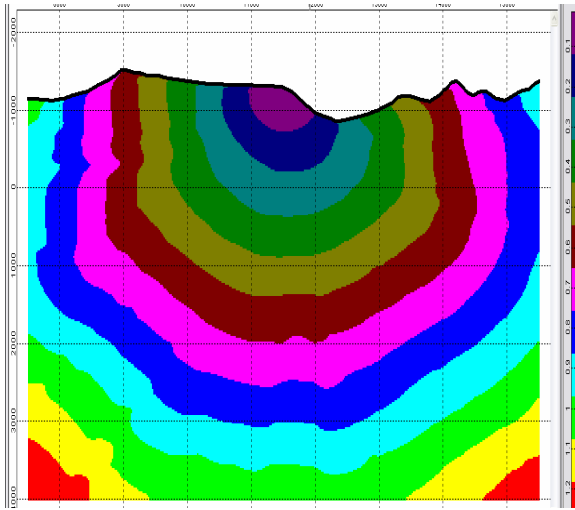


FIG. 12a. Plot of the First Arrivals Time field (Elastic modeling).

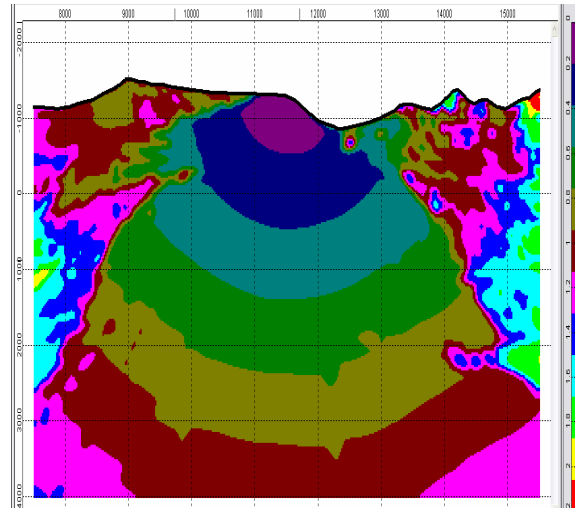


FIG. 12b. The Maximum Energy Time field (Elastic modeling).

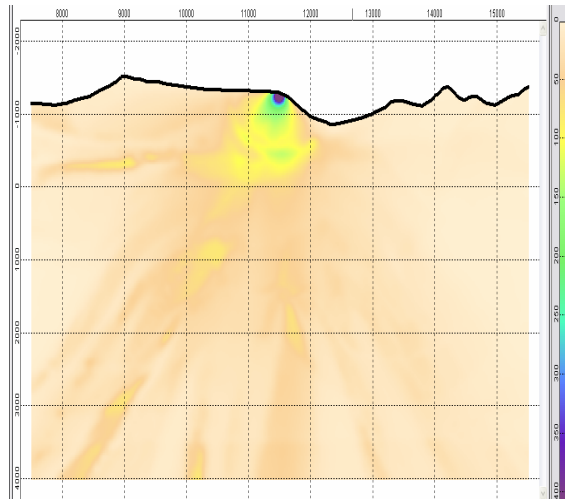


FIG. 13a. The Green's function for Kirchhoff migration of the energy field of a downgoing wave using first arrival times.

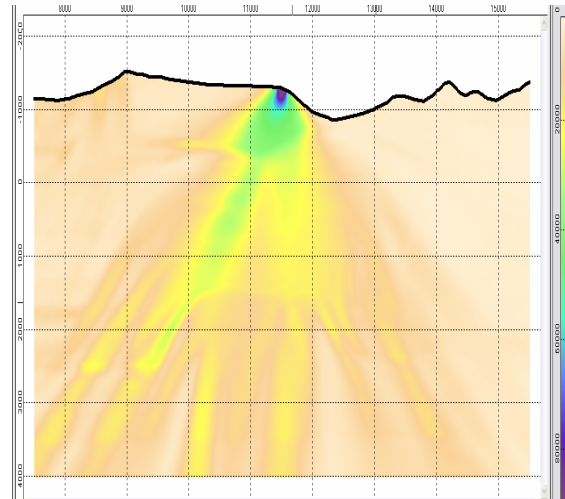


FIG. 13b. The Green's function for Kirchhoff migration of the energy field of a downgoing wave using the maximum energy time field.

PRESTACK DEPTH MIGRATION PROCESSING OF FIRST ARRIVALS VERSUS MAXIMUM ENERGY

It is noticeable that when using a maximum energy time field, part of the V-shaped shallow syncline is revealed, along with some deeper horizons. Unlike the first arrival image, there is no phase shift happening by using the maximum energy.

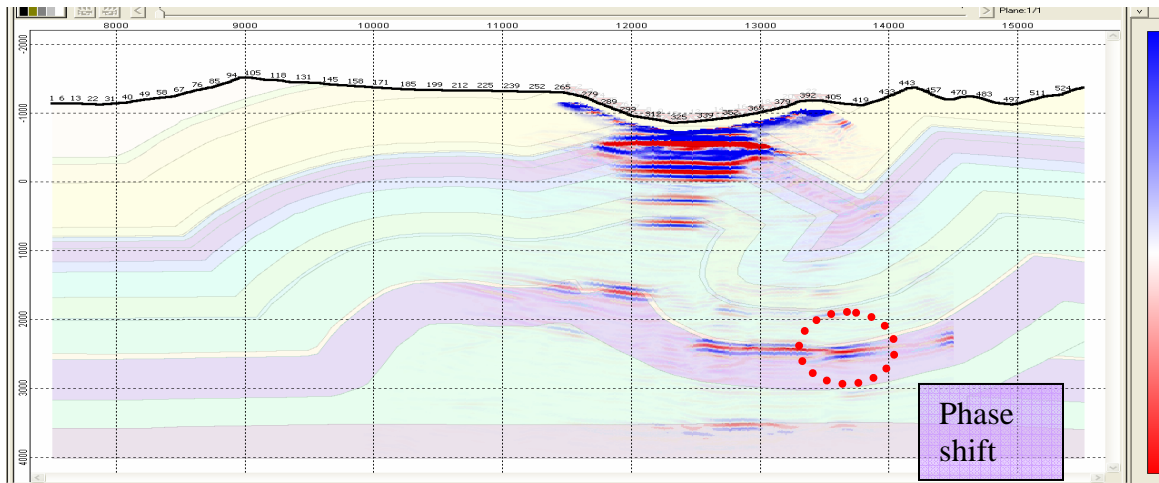


FIG. 14. Prestack depth migration processing using first arrivals time field – migration aperture 5000 m (Elastic modeling) 23 Shot (90 m) - 534 Receivers (15 m) -25 Hz Ricker.

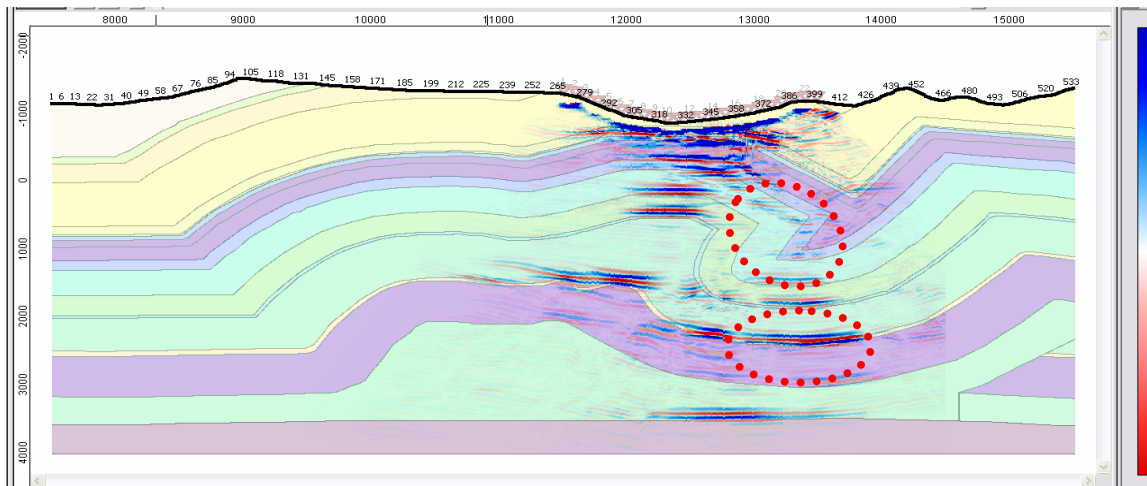


FIG. 15. Prestack depth migration processing using the maximum energy time field – migration aperture 5000 m (Elastic modeling) 23 Shot (90 m) - 534 Receivers (15 m) -25 Hz Ricker. The imaging potential of this method can be predicted.

THE COMPUTATION TIME AND DISK REQUIREMENTS

Elastic modeling requires more time and memory capacity than the acoustic modeling method, and the fine source/receiver intervals will also require more computation time to produce synthetic shot gathers, time field, energy fields, and snapshots for the survey parameters indicated (Table 3). Running the elastic modeling experiment required sixty three days, using one thousand and sixty seven shots with five meter group intervals and fifteen meters source intervals. Computation time is also required to migrate the shot records.

Table 3a. Summary of one shot record run time.

Modeling	Group Interval (m)	Computation Time	Memory (Mb)
Acoustic	5	00:30:09	45.2
	10	00:26:32	45.2
	15	00:27:43	45.2
	30	00:27:11	45.2
Elastic	5	01:26:51	108
	10	01:24:59	108
	15	01:23:57	108
	30	01:23:46	108

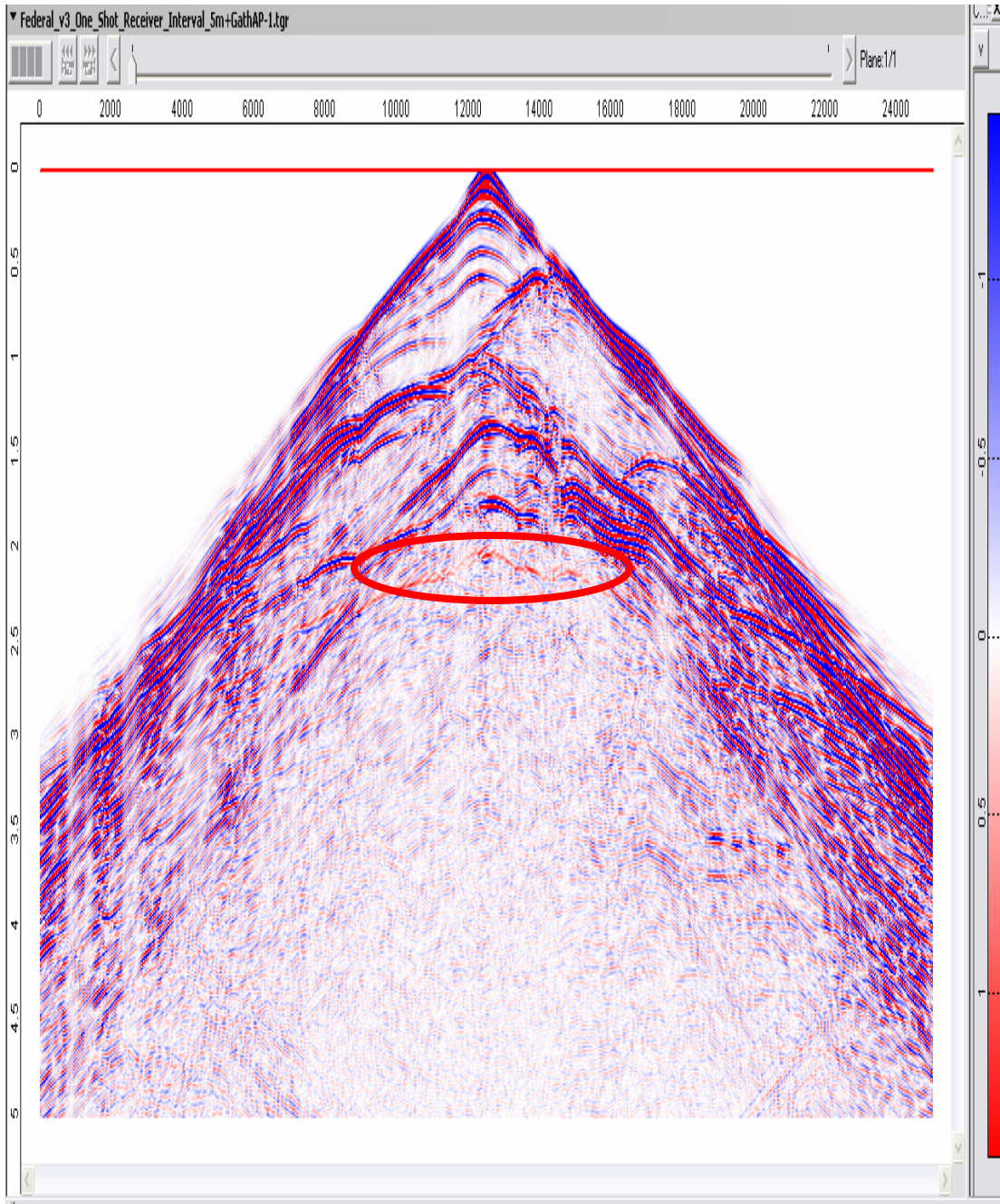
Table 3b. Summary of Tesseral Model Run Time - PC with 1/2 Gb Ram.

Station/ SHPT Spacing	Time estimate for a 16 km line						
	# Shots	Acoustic			Elastic		
		Hours	Days	Disk (GB)	Hours	Days	Disk (GB)
30/180	89	40.3	1.7	4.0	124	5.2	9.6
15/90	178	82.2	3.4	8.0	249	10.4	19.2
10/60	267	118.1	4.9	12.1	378	15.8	28.8
15/45	356	178.9	7.5	16.1	509	21.2	38.4
5/15	1067	536.2	22.3	48.2	1527	63.6	115.2

SHOT RESPONSE USING ACOUSTIC/ELASTIC MODELING

One shot was placed at the surface to illustrate the response of the geologic model to the propagating waves using compressional velocities, shear velocities and densities. Direct wave arrivals and reflected events were recorded, and the effect of shear waves was present on the shot response using the elastic modeling. As well, the deeper event circulated on the acoustic modeling figure has been hidden because of the hatched noise pattern. (Figure 16)

Shot response - Acoustic Modeling



Shot response - Elastic Modeling

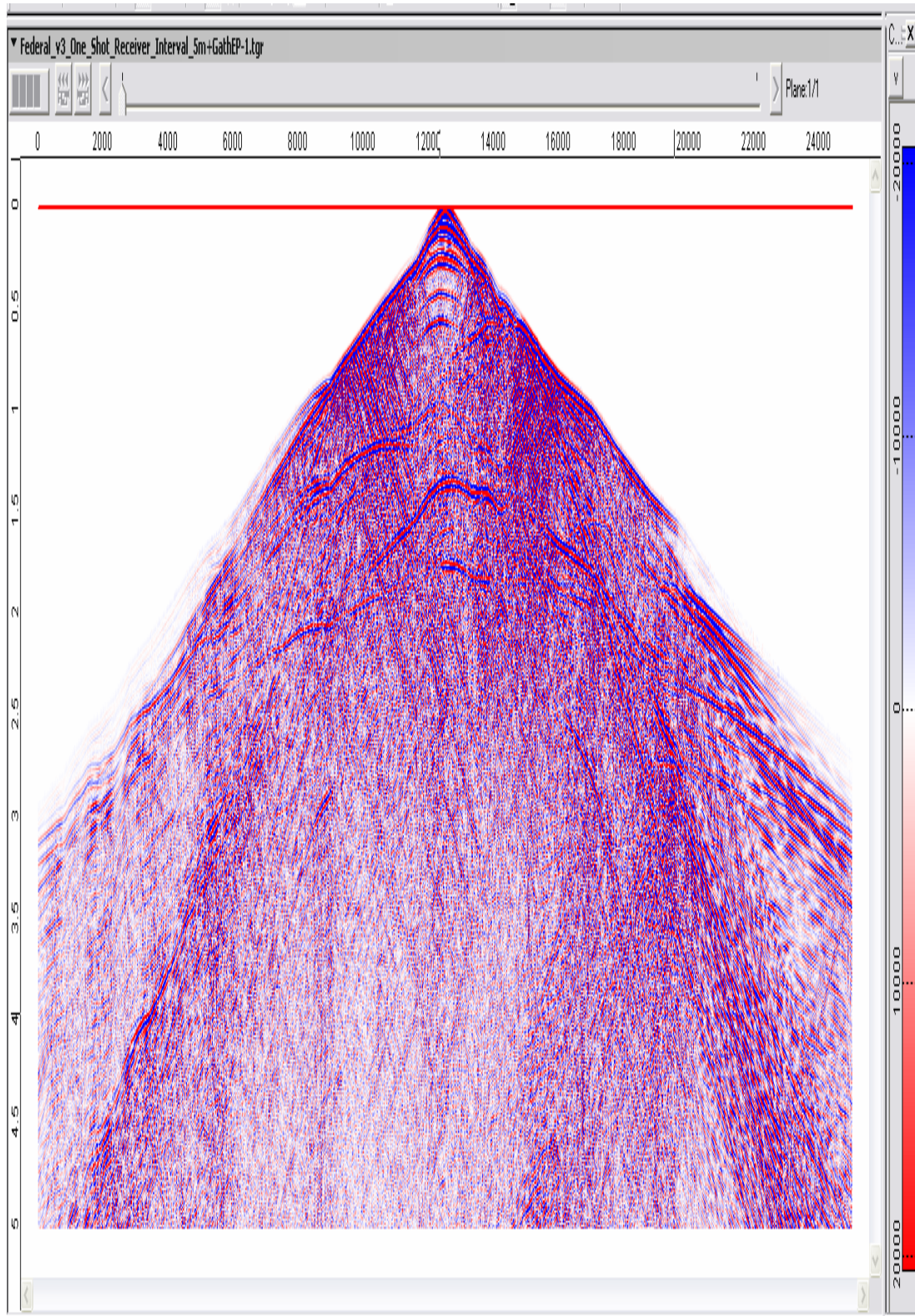


FIG.16. Shot response – acoustic/elastic modeling.

PRESTACK KIRCHHOFF DEPTH MIGRATION USING ACOUSTIC/ELASTIC MODELING

It was anticipated that we wouldn't be able to see the fault plane, but rather the discontinuities in the reflection, because the severe dips impose severe limits on our field techniques. In other words, only horizons with less than 30 degrees dip angle or so are expected to be imaged. However, in the experiment illustrated in Figure 17 we can see the thrust along with the other steep horizons have been imaged.

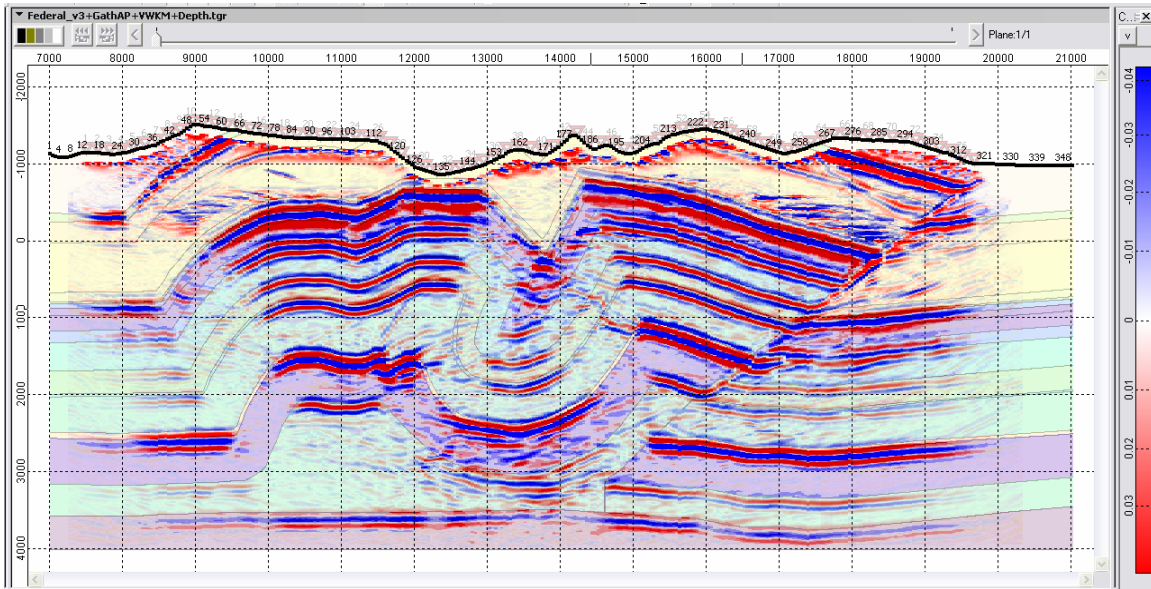


FIG. 17a. Prestack depth migration (acoustic modeling) with migration aperture 5000 m – Section length = 21 km, section depth = 6 km, 77 Shots (160 m) - 351 Receivers (40 m) -25 Hz Ricker- Elapsed Time 49:50:48.

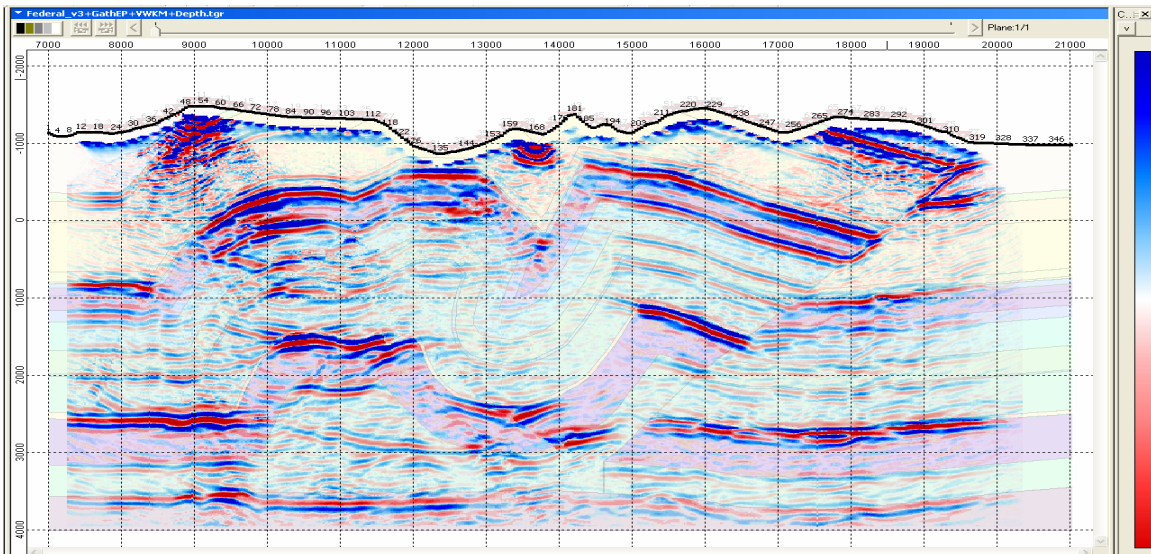


FIG. 17b. Prestack depth migration (elastic modeling) with migration aperture 5000 m – Section length = 21 km, section depth= 6 km, 77 Shots (160 m) – 351 Receivers (40 m) – 25 Hz Ricker - Elapsed Time 97:49:54.

RESULTS

Comparison between two pre-stack Kirchhoff depth migrations of the synthetic model of the Husky Federal line H98-154 in North Eastern B.C. were done by two different methods of generating traveltimes as well as different modeling algorithms. Maximum energy time field calculations revealed that parts of the syncline formations were more difficult to image using the first arrival method. Additionally, finer source & geophone intervals should give better results; but because of computation time and disk space limitations, this portion of the project will be done at a later time. The elastic modeling requires more time and disk space, while producing the hatched patterns in the shot gathers. The maximum energy time field calculated from the twenty three shots showed the general shape of the deeper part of the model where the energy originates.

CONCLUSIONS

The imaging potential of prestack depth Kirchhoff migration using maximum energy times can be predicted; and the opportunity exists to greatly enhance the accuracy of interpretation in structurally complex areas. One should take care in order to avoid increasing computation time, by considering the above-mentioned summary table of estimated run times, which can help economically justify using the method. Care must be taken to use enough apertures so that the point diffractors do not distort into frown artifacts on a depth section. Finally, it is our intention to demonstrate the use of prestack depth Kirchhoff migration, using maximum energy times, to process the Husky line with a wide variation in surface elevations and complex geological deformation pattern.

ACKNOWLEDGEMENTS

The authors wish to thank Larry Mewhort, David Emery, Bart Scott, Bill Bradley and Craig Lamb for sponsoring the project and their helpful advice.

We express our appreciation to Husky Energy and MITACS for funding this project and the sponsors of CREWES.

REFERENCES

Nichols D.E., 1996, Maximum energy traveltimes calculated in the seismic frequency band: *Geophysics*, **61**, 253-263.